The Astrophysical Journal Letters, 851:L17 (6pp), 2017 December 10 https://doi.org/10.3847/2041-8213/aa9e0a

The Mechanism for the Energy Buildup Driving Solar Eruptive Events

K. J. Knizhnik[1], S. K. Antiochos, C. R. DeVore, and P. F. Wyper[2]
Heliophysics Science Division, NASA Goddard Space Flight Center, Greenbelt, MD 20771, USA; kalman.knizhnik.ctr@nrl.navy.mil
Received 2017 October 30; revised 2017 November 17; accepted 2017 November 28; published 2017 December 8

Abstract

The underlying origin of solar eruptive events (SEEs), ranging from giant coronal mass ejections to small coronal-hole jets, is that the lowest-lying magnetic flux in the Sun's corona undergoes continual buildup of stress and free energy. This magnetic stress has long been observed as the phenomenon of "filament channels:" strongly sheared magnetic field localized around photospheric polarity inversion lines. However, the mechanism for the stress buildup—the formation of filament channels—is still debated. We present magnetohydrodynamic simulations of a coronal volume that is driven by transient, cellular boundary flows designed to model the processes by which the photosphere drives the corona. The key feature of our simulations is that they accurately preserve magnetic helicity, the topological quantity that is conserved even in the presence of ubiquitous magnetic reconnection. Although small-scale random stress is injected everywhere at the photosphere, driving stochastic reconnection throughout the corona, the net result of the magnetic evolution is a coherent shearing of the lowest-lying field lines. This highly counterintuitive result—magnetic stress builds up locally rather than spreading out to attain a minimum energy state—explains the formation of filament channels and is the fundamental mechanism underlying SEEs. Furthermore, this process is likely to be relevant to other astrophysical and laboratory plasmas.

Key words: Sun: filaments, prominences

Supporting material: animation

1. Introduction

The solar corona has long been observed to exhibit frequent ejections of matter and magnetic field into interplanetary space, usually accompanied by bursts of ultraviolet (UV) to X-ray radiation. These solar eruptive events (SEEs) range from 10^{32} ergs or more for a major coronal mass ejection (CME)/eruptive flare to 10^{27} ergs or less for a coronal-hole jet (e.g., Raouafi et al. 2016). Given their short timescales—tens of minutes for large CMEs/flares to minutes for jets—SEEs are widely believed to represent the explosive release of magnetic free energy stored in the corona, specifically in highly stressed fields of filament channels (FCs). These structures have long been postulated to be the source of large SEEs such as CMEs/eruptive flares (e.g., Forbes 2000; Mackay et al. 2010), but recent observations indicate that even small jet-like eruptions result from the release of magnetic energy stored in mini-filaments (Sterling et al. 2015; Kumar et al. 2017). Consequently, understanding how FCs form is equivalent to understanding how the energy for SEEs accumulates in the corona, one of the most important problems in heliophysics.

FCs consist of strongly sheared magnetic flux that is highly localized about a polarity inversion line (PIL; e.g., Mackay 2015). They are ubiquitous throughout the corona, occurring along all types of PILs, from the strongest active regions to the quietest high-latitude regions bordering polar coronal holes. It is generally believed that an FC will eventually develop at every large-scale PIL (Mackay 2015). Cool ($\sim 10^4$ K) material frequently (but not always) collects in FCs to form the filaments/prominences that have been observed for centuries. Numerous observations, including measurement of vector magnetic fields at the photosphere (e.g., Rust 1967; Leroy et al. 1983; Martin 1998) and direct measurement of vector fields in prominences (Casini et al. 2003; Kuckein et al. 2012), have established definitively that FC field lines are long and greatly stretched parallel to the PIL, rather than short and perpendicular. These long "sheared" magnetic field lines are also mandated theoretically to support dense prominence material against gravity (Tandberg-Hanssen 1995). Importantly, FCs are the only places where the corona is strongly non-potential; the rest of the closed-field corona is typically observed to consist of smooth, laminar, quasi-potential loops (e.g., Schrijver et al. 1999).

Given the one-to-one association between FCs and PILs, the two classic models for FC formation invoke the property unique to PILs that flux emerges and cancels there. In the emergence model, magnetic shear forms along a PIL due to the large-scale emergence of a subsurface twisted flux rope. The idea is that a horizontal twisted flux rope can emerge only partially, the concave-up portion below the central axis remaining trapped below the photosphere by the weight of the dense plasma. In this case, the highly twisted outer flux appears as a high-lying quasi-potential coronal arcade, while the axial inner flux appears as low-lying sheared field almost parallel to the PIL. Numerical simulations confirm that emergence generally results in sheared flux localized along PILs, similar to observed FCs (e.g., Fan 2001; Manchester 2001; Magara & Longcope 2003; Archontis et al. 2013; Leake et al. 2013). Large-scale flux emergence occurs only in young active regions, whereas FCs form on all PILs, even where flux is not emerging. The recent jet observations demonstrate, in particular, that mini-filaments do not require flux emergence (Sterling et al. 2015; Kumar et al. 2017). Consequently, emergence cannot explain most FCs.

In the cancelation model, the coronal magnetic field acquires large-scale shear due to differential rotation or other large-scale

[1] Current Address: Space Science Division, Code 7683, Naval Research Laboratory, Washington, DC 20375-5337, USA.
[2] Current Address: Department of Mathematical Sciences, Durham University, Stockton Road, Durham DH1 3LE, UK.

motions and/or to active-region emergence. This shear convects with the field toward PILs, where positive and negative fluxes reconnect at the photosphere and submerge while the shear remains in the corona and accumulates at the PILs (van Ballegooijen & Martens 1989; Mackay et al. 2010). The drawback with the cancelation theory is that outside of filaments, the coronal magnetic field exhibits only small stress. Many high-resolution observations (e.g., Schrijver et al. 1999) have shown that coronal loops are laminar and not far from their current-free state, as expected theoretically (e.g., Parker 1983). Both theory and simulations demonstrate, however, that when low-shear flux reconnects systematically along PILs, the resulting field lines are highly twisted (van Ballegooijen & Martens 1989; Mackay et al. 2010). This exact process occurs in the well-known two-ribbon flare, where systematic reconnection of coronal flux along an X-line produces the highly twisted flux rope observed as an interplanetary CME (e.g., Longcope 1996; Qiu et al. 2007; Gopalswamy et al. 2017). Strong twist, however, is not observed in filaments (e.g., Lin et al. 2005; Vourlidas et al. 2010) or anywhere else in the corona, except as the aftermath of flare reconnection. A mechanism that explains observed FCs must produce strong shear at *all* PILs, but with minimal twist.

A model that satisfies these challenging requirements was proposed by Antiochos (2013). This "helicity condensation" model builds upon the standard processes postulated for quasi-steady coronal heating (e.g., Klimchuk 2006). First, stress is injected into the coronal magnetic field by turbulent cellular convective motions and continual emergence and submergence of small-scale flux throughout the photosphere, the so-called magnetic carpet (Title 2000). Reconnection then releases free energy stored in this small-scale stress, heating the plasma and keeping the coronal field outside of filaments laminar, as observed (Schrijver et al. 1999).

Helicity condensation theory adds to these well-known processes the key concept of helicity conservation. Magnetic helicity is the topological measure of field-line linkages (e.g., Berger & Field 1984; Finn & Antonsen 1985; Moffatt & Ricca 1992). The all-important property of helicity is its conservation under magnetic reconnection (Woltjer 1958), which imposes strict constraints on the evolution and equilibrium state of the coronal magnetic field (e.g., Taylor 1974, 1986). If the stress injected into the corona contains net magnetic helicity, this helicity cannot be destroyed by reconnection and, therefore, must accumulate. The evidence favoring net coronal helicity injection is compelling. Many observations have shown that in the Sun's northern hemisphere, large-scale structures such as active regions, filaments, and supergranular flows predominantly have negative helicity, whereas those in the southern have positive (Martin et al. 1992; Rust & Kumar 1994; Zirker et al. 1997; Pevtsov et al. 2003). A detailed analysis of erupting filaments indicates that the helicity preference may reach 90% (Ouyang et al. 2017). Helicity condensation theory argues that if this hemispheric preference extends down to the scales of convective flows and flux emergence, then the helicity associated with small-scale stress injected into the corona will be transformed by reconnection into large-scale magnetic shear localized about PILs (Antiochos 2013).

This conjecture has been tested numerically (Knizhnik et al. 2015, 2017; Zhao et al. 2015), but only within a simplified Parker (1972) corona, which consists of an initially uniform vertical field between two horizontal planes that represent the photosphere. Small-scale flows on these planes injected free energy and helicity into the system. Although the Parker model is useful for studying coronal heating, its major shortcoming for testing helicity condensation is that there is no PIL. The simulations instead divided the domain into an inner region driven by photospheric flows and an outer undriven region; the boundary between was assumed to represent the PIL. The photospheric driving and coronal reconnection did cause the magnetic stress to accumulate at this "PIL." However, such evolution is also expected from energy arguments. Simple energy minimization demands that any net magnetic stress should spread out as much as possible into the undriven region. Hence, although the Parker-model simulations provide important insight into the process of helicity condensation, they cannot definitively account for the observed FC formation and energy buildup that is responsible for SEEs. We describe below, for the first time, a rigorous demonstration of helicity condensation in a realistic coronal system with a true PIL.

2. Numerical Model

For this Letter, we solved the ideal magnetohydrodynamics equations in Cartesian coordinates using the Adaptively Refined MHD Solver (DeVore & Antiochos 2008). Magnetic reconnection occurs in the simulations due to numerical diffusion at locations where the current density develops grid-scale structure. The domain size is $[0,\ L_x] \times [-L_y,\ +L_y] \times [-L_z,\ +L_z]$, where x is the vertical direction (normal to the photosphere), $L_x = 2.0$, and $L_y = L_z = 3.5$. We employed zero-gradient conditions at all six boundaries at all times. The bottom boundary was closed and line-tied, so field lines moved only in response to imposed boundary flows described below. This emulates the slow driving at the dense photosphere, overriding the response to coronal magnetic and other forces. All other boundaries were open and free slip, so that both plasma and magnetic field moved along and across each boundary.

The initial plasma parameters in our dimensionless simulations were $\rho_0 = 1$, $P_0 = 1$, so the sound speed $c_s = (\gamma P_0/\rho_0)^{1/2} = 1.3$ for $\gamma = 5/3$. For the prescribed initial magnetic field, defined below, the Alfvén speed $c_{A0} = B_0/(4\pi\rho_0)^{1/2}$ ranged from 1.4 to 21.2, and the plasma beta (ratio of thermal to magnetic pressure) $\beta_0 = 8\pi P_0/B_0^2$ ranged from 4×10^{-3} to 1. The regime $\beta \ll 1$ models a magnetically dominated plasma such as the corona. The regions where $\beta \approx 1$ are mostly in the corners of our domain; the amount of moderate-beta plasma is minimal and does not affect our results.

The initial magnetic state superposes a uniform vertical background field, $B_0 = -4$, and a potential bipolar sunspot whose magnetic field normal to the photospheric boundary ($x = 0$) is

$$B_{ss}(r) = \frac{B_+}{2}\left\{1 - \tanh\left(\frac{r^2 - r_+^2}{\lambda_+^2}\right)\right\} - \frac{B_-}{2}\left\{1 - \tanh\left(\frac{r^2 - r_-^2}{\lambda_-^2}\right)\right\}. \quad (1)$$

Here, $r = (y^2 + z^2)^{1/2}$ is the cylindrical radial coordinate on the plane; $B_+ = 60$, $\lambda_+ = 0.5$, and $r_+ = 2$; and $B_- = 15$,

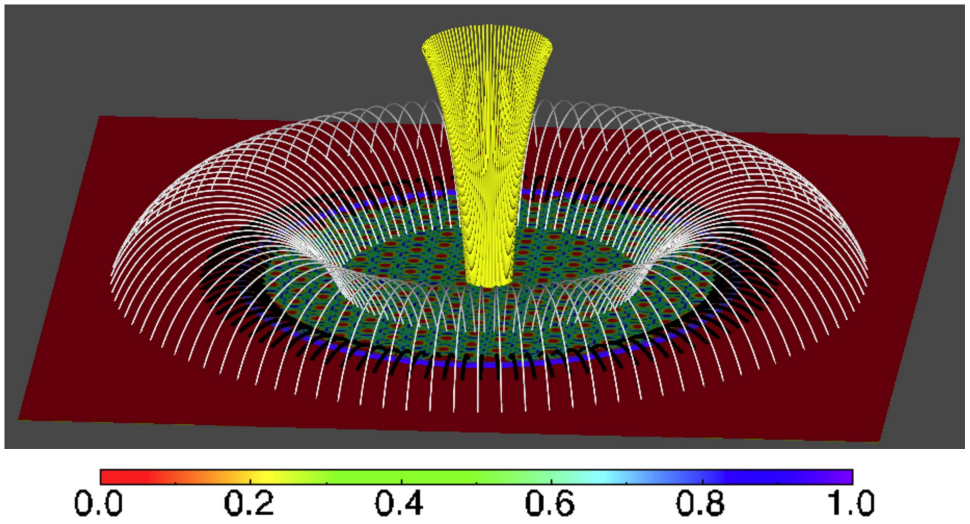

Figure 1. Simulation setup showing closed, line-tied field lines (white and black) traced from the bottom boundary crossing the circular PIL (blue), and open, free-slip field lines (yellow) traced from the top boundary. Bottom boundary shading shows velocity magnitude due to driving inside the PIL.

$\lambda_- = 1$, and $r_- = 4$. The PIL is located just beyond $r = r_+ = 2$.

Figure 1 shows the simulation domain along with some representative initial field lines. Black and white field lines in Figure 1 are tied at both ends corresponding to the closed corona, whereas yellow lines are open at the top ends corresponding to field that is open to the solar wind. The flux distribution of Figure 1 is clearly far simpler than observed photospheric flux distributions, but our system nevertheless captures the essential features of a bipolar field with closed and open field lines in the corona and a PIL on the photosphere.

To model photospheric convection, we placed 199 convective cells on the bottom boundary, arranged as shown in Figure 1. The flows fill the inner, positive-polarity region except for a tiny band about the PIL. Applying flows at the PIL itself would result in mixing positive and negative flux down to the grid scale, making it impossible to resolve numerically the magnetic evolution there. Even with our restricted driving, the numerical resolution near the PIL becomes marginal, resulting in the small ($\sim$10%) violation of helicity conservation discussed below (Figure 2). Furthermore, mixing fluxes of opposite polarity would require a rigorous treatment of flux cancelation with submergence at the PIL, which is beyond the scope of our model and this Letter. The slow cellular motions were imposed only within the central polarity of the sunspot, for simplicity. The injected magnetic stress, however, is redistributed by fast Alfvén waves throughout *all* the closed flux, as shown below (Figure 3). Driving the outer-polarity region directly would only increase the number of convection cells and the rates of helicity injection and generation of small-scale structure.

By design, the convective flows preserve the vertical flux distribution, B_x, on the surface, as described in detail elsewhere (Knizhnik et al. 2015). Each cell has radius $a_0 = 0.125$ and peak linear velocity $v_{\max} = 1.2$, about 5% of the maximum Alfvén speed. The flows turn on from zero, and then turn off back to zero, at fixed period $t = 0.572$. In some cases, we used these pauses in the flow either to rotate the entire pattern of convective cells about the sunspot center or to flip the sense of rotation (clockwise or counter) according to a random probability assigned to each cell.

We calculated the magnetic helicity in our domain in two ways (Knizhnik et al. 2015): by evaluating the gauge-independent, instantaneous volume integral for H due to Finn & Antonsen (1985) and by time-integrating the rate of helicity gain/loss, dH/dt, which was derived from the Finn–Antonsen expression and consists of surface integrals of helicity fluxes through all six boundaries. The results are shown as the red and black curves, respectively, in Figure 2. We found that about 10% of the helicity flux entering the bottom exited the top, in accordance with the ratio of areas of open field (yellow lines in Figure 1; $\approx$19 convection cells) to closed field (black/white lines; $\approx$180 cells). Negligible helicity fluxes exited the side boundaries. After 90 cycles, the accumulated helicity falls short of the net injected helicity, also by about 10%. This represents a small loss due to grid-scale diffusion, but verifies that the evolution of our system is dominated by helicity-conserving reconnection.

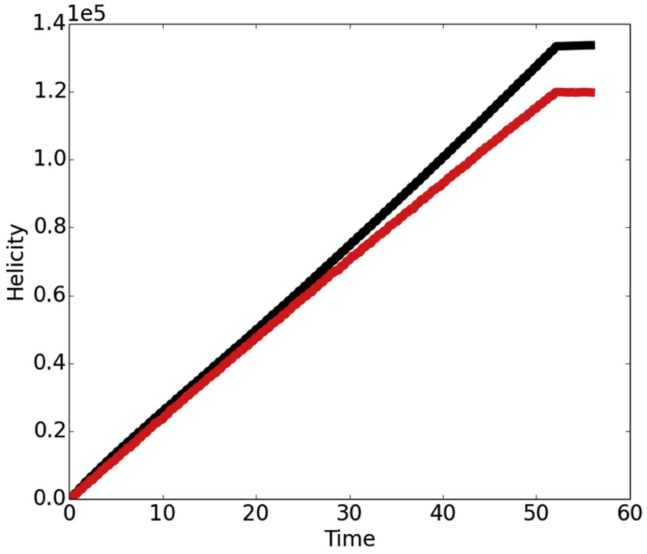

Figure 2. Accumulated magnetic helicity injected/lost through the boundaries (black) and stored in the volume (red).

3. Results

To test the helicity condensation mechanism for FC formation, we performed several simulations with varying assumptions on the driving flows. In the case shown below,

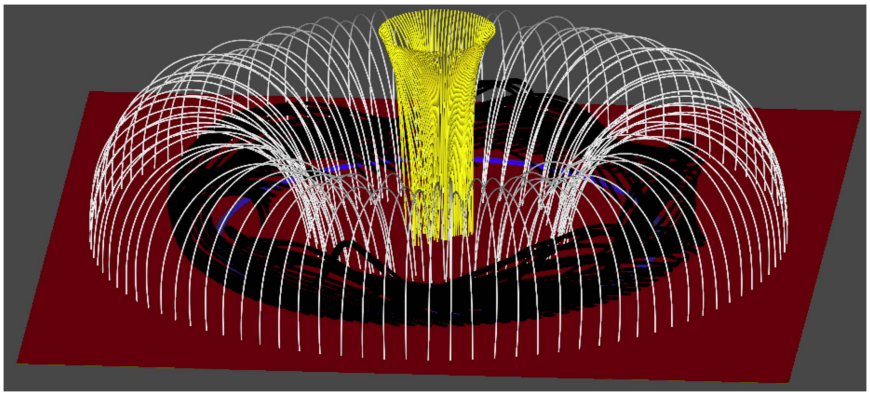

Figure 3. End state of Figure 1 after 90 randomly shifted rotation cycles and 7.5 relaxation cycles (see the associated animation). (An animation of this figure is available.)

each small-scale flow was imposed for a maximum rotation of π, then the whole flow pattern was shifted by a random angle and a new rotation applied. This procedure was performed for 90 cycles of rotation, followed by 7.5 cycles with no driving to allow the system to relax. Due to the random pattern shifting, the driving motion is truly chaotic, as is the driving expected from the solar convective flows and magnetic carpet (Duvall & Gizon 2000; Title 2000). We also investigated cases where the flow pattern was held fixed throughout the simulation and obtained results quantitatively similar to the corresponding random-driving cases. To maximize the helicity injection rate and minimize the computational time, all flows in the simulation shown below were assigned the same (clockwise) sense of rotation. We also investigated cases in which every small-scale flow was assigned a probability governing the sense of rotation for each cycle. For example, assigning a 50% probability of clockwise versus counterclockwise produces zero net helicity injection. This case did not form an FC at the PIL nor generate continuous free-energy buildup. Assigning a 75% clockwise probability and 25% counter leads to results essentially identical to those below, except that the helicity and energy buildup rates were 50% smaller. These results demonstrate that the flow pattern details are not important for FC formation. The only requirements are that net helicity is injected and reconnection occurs quasi-chaotically throughout the corona.

Figure 3 shows the end state of our randomly shifted system (the detailed qualitative evolution can be seen in the accompanying animation). This result is an amazing example of self-organization. First, note that the yellow open lines are almost unchanged from their initial state in Figure 1. This is expected because any stress injected onto these lines simply propagates out of the system. The white field lines near the center of the closed-field region are somewhat changed from their initial state, but far less than expected under ideal evolution. If there were no coronal reconnection, the footpoint driving for this random case would produce a completely tangled, twisted mess; the fixed-flow case, in contrast, would produce a set of parallel, highly twisted (≈45 turns), small flux tubes. In both cases, we find instead that the white field lines are smooth and laminar—similar to their initial potential state, except that they bulge upward substantially—appearing very much like the loops that are commonly observed in the closed corona (Schrijver et al. 1999). Our results demonstrate that small-scale "chaotic" reconnection can explain these observations, despite the complex driving from photospheric convection and small-scale flux emergence.

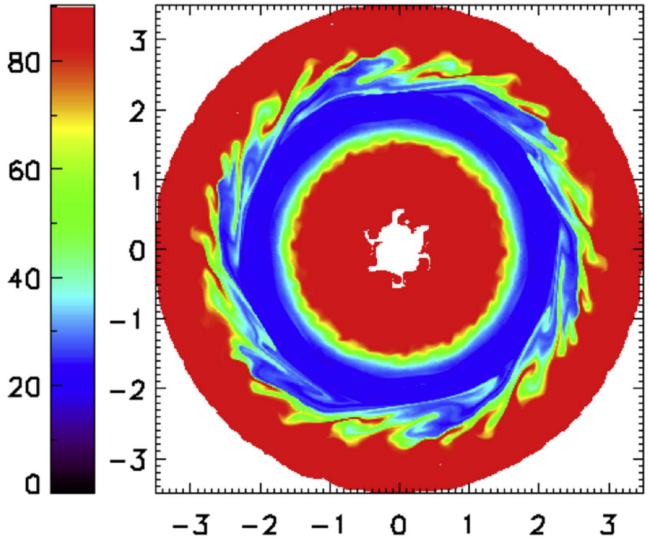

Figure 4. Shear angle in degrees (color shading) between the footpoints of closed field lines and the PIL. White areas denote open field lines.

The black field lines near the PIL, on the other hand, are drastically changed from their initial state. They are now greatly stretched along the PIL, with a ratio of parallel to perpendicular field components as large as ≈5. These lines have exactly the properties required to explain FCs. They are strongly sheared and roughly parallel to the PIL, possess local depressions ("dips") in the corona, and have at most one-half turn of internal twist. To quantify the shear, we connected the footpoints of each closed field line with a straight line on the bottom boundary and measured the angle between that straight line and the PIL where the two cross. The resulting shear angle, which initially is 90° everywhere but decreases to and saturates at about 20° within the FC, is plotted in Figure 4. The FC is as narrow as it can be, one convection-cell diameter wide on each side of the PIL (Antiochos 2013; Knizhnik et al. 2015), while its height increases as the shear flux accumulates. We emphasize that this smooth, sheared FC structure was obtained even though all the driving motions were purely rotational, for 90 half-turns, with no large-scale coherent displacement. This point is critically important. The results shown arise solely from the effects of coronal reconnection and helicity conservation and, therefore, are completely general. The same structure would result for any form of small-scale complex driving, as long as net helicity is injected into the system. We

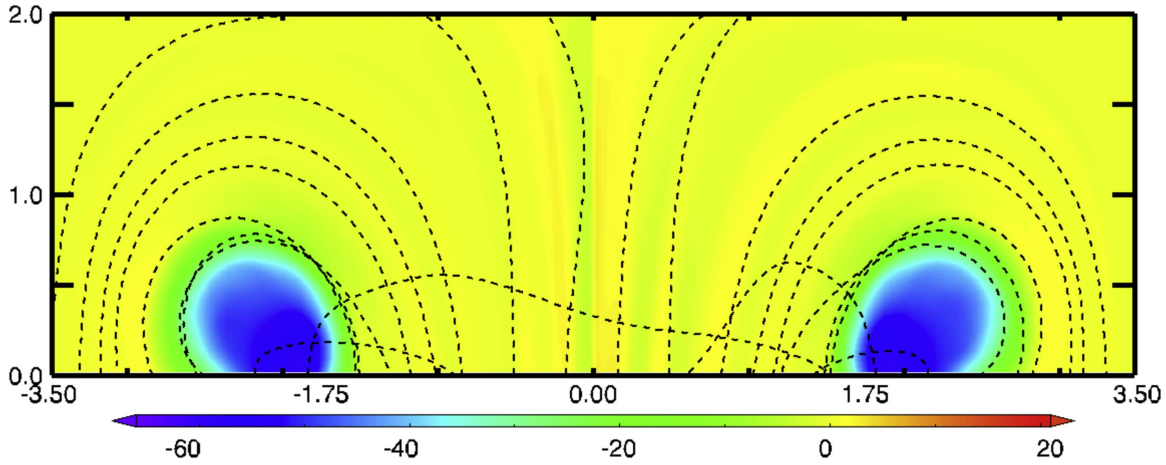

Figure 5. Azimuthal field (color shading) through a vertical plane between the top and bottom boundaries with selected field lines (dashed) projected onto the plane.

expect, therefore, that FCs and the energy buildup leading to eruptions will occur in any corona-like system, including the atmospheres of late-type stars, accretion disks, etc.

To show that the state above is ripe for magnetic eruption, we plot in Figure 5 the shear flux through a vertical plane. Selected field lines that sample both open and closed fluxes, and both the FC and its overlying restraining field, also are shown. The low-lying flux bulges outward to minimize the magnetic pressure associated with its strong shear, but it is held back by the magnetic tension of the overlying unsheared flux. This is exactly the force balance believed to underlie all CMEs/flares (Priest 2014) and even coronal jets (Wyper et al. 2017). However, we believe it unlikely that this Cartesian configuration will ever erupt, even with continued cellular driving, due to the large energy required to open all the flux overlying the FC. On the Sun and in spherical simulations, on the other hand, the FC and overlying flux can expand radially, not just vertically, thereby lowering their energy. Hence, we conjecture that the spherical equivalent of our present configuration could erupt, but this remains to be demonstrated.

It is important to understand physically why the magnetic state of Figures 3–5 develops. Obviously, it does not minimize the energy. For a "turbulently" reconnecting system in which helicity conservation is the only constraint, the minimum energy state is a linear force-free field (FFF; e.g., Taylor 1974; Heyvaerts & Priest 1984). Our system is close to force-free, but the stresses (i.e., electric currents) are tightly concentrated near the PIL rather than distributed uniformly throughout the field as in linear FFFs. Indeed, the only linear FFF appropriate to our system is the potential (current-free) state of Figure 1, because the open flux cannot support steady electric currents. Clearly, our system has additional constraints beyond helicity conservation, most likely due to the photospheric line-tying (e.g., Antiochos et al. 2002).

Our simulation results can be understood, instead, in terms of the well-known inverse cascade of helicity in turbulence theory, but with a curious twist. An inverse cascade implies that helicity should "condense" at the system's largest spatial scale, its boundary (Biskamp 1993). The system of Figure 1 has two boundaries that define the amount of closed flux: an inner circle separating open (yellow) and closed (white) field lines, and the blue PIL. The former corresponds to the largest spatial scale because the longest field lines occur there. However, any helicity that condenses there simply propagates away as Alfvén waves along infinitely long open lines, thereby minimizing the energy as well. Our striking result is that helicity also condenses onto the other boundary, the PIL, even though it corresponds initially to the system's shortest field lines. Helicity condensation at this boundary continuously forms a filament channel and builds up free energy, which can be removed only through ejection. We conclude, therefore, that the highly counterintuitive mechanism of helicity condensation may finally explain why the solar corona continually undergoes magnetic eruption.

Our work was supported by NASA's LWS, H-SR, NESSF, NPP, and HEC programs.

ORCID iDs

K. J. Knizhnik https://orcid.org/0000-0002-2544-2927
S. K. Antiochos https://orcid.org/0000-0003-0176-4312
C. R. DeVore https://orcid.org/0000-0002-4668-591X
P. F. Wyper https://orcid.org/0000-0002-6442-7818

References

Antiochos, S. K. 2013, ApJ, 772, 72
Antiochos, S. K., Karpen, J. T., & DeVore, C. R. 2002, ApJ, 575, 578
Archontis, V., Hood, A. W., & Tsinganos, K. 2013, ApJ, 778, 42
Berger, M. A., & Field, G. B. 1984, JFM, 147, 133
Biskamp, D. 1993, Nonlinear Magnetohydrodynamics (New York: Cambridge Univ. Press)
Casini, R., Lopez Ariste, A., Tomczyk, S., & Lites, B. W. 2003, ApJL, 598, L67
DeVore, C. R., & Antiochos, S. K. 2008, ApJ, 680, 740
Duvall, T. L., Jr., & Gizon, L. 2000, SoPh, 192, 177
Fan, Y. 2001, ApJL, 554, L111
Finn, J., & Antonsen, T. 1985, CoPPC, 9, 111
Forbes, T. G. 2000, JGRA, 105, 23153
Gopalswamy, N., Yashiro, S., Akiyama, S., & Xie, H. 2017, SoPh, 292, 65
Heyvaerts, J., & Priest, E. R. 1984, A&A, 137, 63
Klimchuk, J. A. 2006, SoPh, 234, 41
Knizhnik, K. J., Antiochos, S. K., & DeVore, C. R. 2015, ApJ, 809, 137
Knizhnik, K. J., Antiochos, S. K., & DeVore, C. R. 2017, ApJ, 835, 85
Kuckein, C., Martinez Pillet, V., & Centeno, R. 2012, A&A, 539, A131
Kumar, P., Karpen, J. T., Antiochos, S. K., et al. 2017, ApJ, submitted
Leake, J. E., Linton, M. G., & Torok, T. 2013, ApJ, 778, 99
Leroy, J. L., Bommier, V., & Sahal-Brechot, S. 1983, SoPh, 83, 135
Lin, Y., Engvold, O., Rouppe van der Voort, L., et al. 2005, SoPh, 226, 239
Longcope, D. W. 1996, SoPh, 169, 91
Mackay, D. H. 2015, in Solar Prominences, ed. J.-C. Vial & O. Engvold (New York: Springer), 355

Mackay, D. H., Karpen, J. T., Ballester, J. L., Schmieder, B., & Aulanier, G. 2010, SSRv, 151, 333
Magara, T., & Longcope, D. W. 2003, ApJ, 586, 630
Manchester, W., IV 2001, ApJ, 547, 503
Martin, S. F. 1998, SoPh, 182, 107
Martin, S. F., Marquette, W. H., & Bilimoria, R. 1992, in ASP Conf. Ser. 27, The Solar Cycle, ed. K. L. Harvey (San Francisco, CA: ASP), 53
Moffatt, H. K., & Ricca, R. L. 1992, RSPSA, 439, 411
Ouyang, Y., Zhou, Y. H., Chen, P. F., & Fang, C. 2017, ApJ, 835, 94
Parker, E. N. 1972, ApJ, 174, 499
Parker, E. N. 1983, ApJ, 264, 642
Pevtsov, A. A., Balasubramaniam, K. S., & Rogers, J. W. 2003, ApJ, 595, 500
Priest, E. R. 2014, Magnetohydrodynamics of the Sun (New York: Cambridge Univ. Press)
Qiu, J., Hu, Q., Howard, T. A., & Yurchyshyn, V. B. 2007, ApJ, 659, 758
Raouafi, N. E., Parsourakos, S., Pariat, E., et al. 2016, SSRv, 201, 1
Rust, D. M. 1967, ApJ, 150, 313
Rust, D. M., & Kumar, A. 1994, SoPh, 155, 69
Schrijver, C. J., Title, A. M., Berger, T. E., et al. 1999, SoPh, 187, 261
Sterling, A. C., Moore, R. L., Falconer, D. A., & Adams, M. 2015, Natur, 523, 437
Tandberg-Hanssen, E. 1995, The Nature of Solar Prominences (Dordrecht: Kluwer)
Taylor, J. B. 1974, PhRvL, 33, 1139
Taylor, J. B. 1986, RvMP, 58, 741
Title, A. 2000, RSPTA, 358, 657
van Ballegooijen, A. A., & Martens, P. C. H. 1989, ApJ, 343, 971
Vourlidas, A., Sanches Andrade-Nuno, B., Landi, E., et al. 2010, SoPh, 261, 53
Woltjer, L. 1958, PNAS, 44, 489
Wyper, P. F., Antiochos, S. K., & DeVore, C. R. 2017, Natur, 544, 452
Zhao, L., DeVore, C. R., Antiochos, S. K., & Zurbuchen, T. H. 2015, ApJ, 805, 61
Zirker, J. B., Martin, S. F., Harvey, K., & Gaizauskas, V. 1997, SoPh, 175, 27